PROCEEDINGS OF SCIENCE

# Performance of the Spanish Infrared Camera onboard the EUSO-Balloon (CNES) flight on August 25, 2014.

**J. F. Soriano , L. del Peral, J. A. Morales de los Ríos, H. Prieto, G. Sáez-Cano**
*Space & Astroparticle (SPAS) Group, UAH, Madrid, Spain*
*E-mails:* jorge.fernandezs@uah.es, luis.delperal@uah.es

**E. Joven, M. Reyes, Y. Martín, J. Licandro**

*Instituto de Astrofísica de Canarias (IAC), Vía Láctea s/n, Tenerife, Spain*

**A. Merino, L. López, J. L. Sánchez***

*GFA. IMA. University of León, León, Spain*

**S. Franchini, E. Roibás**

*IDR, E.T.S.I Aeronáutica y del Espacio, Universidad Politécnica de Madrid, Madrid, Spain*

**M. D. Rodríguez Frías**
*Space & Astroparticle (SPAS) Group, UAH, Madrid, Spain*
*IFIC, CSIC, Universitat de València*
*Dpto. Física Atómica, Molecular y Nuclear, Universitat de València.*

**for the JEM-EUSO Collaboration**

The EUSO-Balloon, pathfinder for the JEM-EUSO Space Mission, was launched during the night of August 25, 2014. The main aim of the flight was to test all the technologies developed for the EUSO (Extreme Universe Space Observatory) Mission under very severe operating conditions (Stratosphere at 40 km altitude), partly representative of the working conditions in ISS. The IR camera onboard EUSO-Balloon is used to obtain the Cloud Top Height (CTH) and cloud coverage in the Field of View (FoV) by using two Long Wave InfraRed (LWIR) bands centered at 10.8 $\mu$m and at 12 $\mu$m. To achieve these objectives a precise control of all the components during the flight is mandatory. The present work is devoted to the evaluation of the spectral and angular response of the microbolometer and filters and a geometrical description of all the components of the IR camera to achieve the proper performances. Once the theoretical study is done, it has to be checked experimentally, determining the involved parameters that have to be taken into account. After this work, we will be able to calculate the CTH of all the clouds in the FOV of the IR camera. CTH is the crucial cloud parameter mandatory for a proper Ultra-High Energy Cosmic Ray (UHECR) and Extremely-High Energy Cosmic Ray (EHECR) analysis.

*The 34th International Cosmic Ray Conference,*
*30 July- 6 August, 2015*
*The Hague, The Netherlands*

*Speaker.

 

PoS(ICRC2015)653

## 1. Introduction

EUSO (Extreme Universe Space Observatory) is a Space Observatory to be placed on board the ISS, with the aim of measuring cosmic rays, at much higher energies than achieved from ground and with much more statistics, using the fluorescence and Cherenkov light emitted along the development of the Extensive Air Shower (EAS) produced by them [1, 2, 3]. As is well established, atmospheric conditions affect the propagation of this light trough the atmosphere until it reaches the telescope. The EUSO atmospheric monitoring system is devoted to monitor these conditions during the measurements of the EAS, to supply the parameters needed to reconstruct the primary particle properties from the measured light [4, 5, 6]. One of the main components of the Atmospheric Monitoring System (AMS) is an infrared camera [7, 8, 9], which measures the thermal radiation produced by clouds to retrieve their Cloud Top Height (CTH), the main scientific and technical return of the infrared camera [10]. In order to improve the CTH retrieval algorithm and Technical Readiness Level (TRL) of the Infrared Camera that the main space mission requires, both from the point of view of the hardware and data analysis, the inclusion in pathfinders of infrared camera prototypes intended to fly in a Space Mission is mandatory. The first of these pathfinders, EUSO-Balloon [11], contained an standalone infrared camera payload, whose composition, measurement principle and performance during the flight is described here.

## 2. The infrared camera

The infrared camera stand-alone payload onboard EUSO-Balloon was allocated inside an Al box attached to the gondola of the balloon. It contained the battery pack, the acquisition electronics, monitoring sensors and the infrared measurement device, which is described here. A brief scheme of the system is shown in Figure 1.

### 2.1 The microbolometer

The Focal Plane Array (FPA) registers the thermal radiation and consists of an ULIS microbolometer with an array of 640 $\times$ 480 pixels. Each one of these pixels is composed by an infrared absorbing material, acting as electrical resistance, and thermally isolated of the rest of the components in each pixel. Under the absorber, an infrared mirror is placed, to increase the amount of radiation deposited in the absorber. While the infrared radiation arrives to the absorber, it warms up, varying the resistance, and producing measurable voltage differences, with a typical

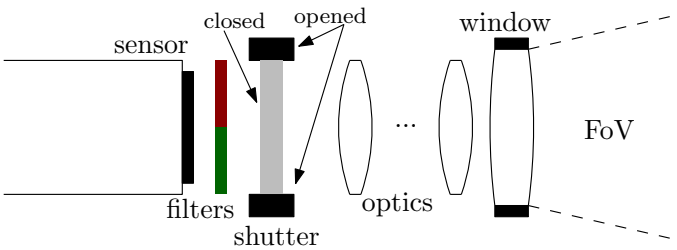


**Figure 1:** Scheme of the infrared camera

response of 3 mV/K. The energy deposited on the absorber can be estimated measuring these voltage variations. The spectral response of the microbolometer is roughly uniform between 8 $\mu$m and 12 $\mu$m.

The response of each pixel depends, among many other parameters, on the Silicon substrate temperature placed under the infrared mirror. In order to achieve a better performance, the FPA includes a thermoelectric cooler, to keep this temperature constant. The other parameters to be tuned affect to the readout integrated circuit and to how it reads and processes the signal from each pixel.

### 2.2 The bispectral filter of the infrared camera

A dual band filter is placed just in front of the FPA. The two bands of the filter are, as shown in Figure 2, centred roughly in 10.8 $\mu$m and 12 $\mu$m.

Both bands are physically separated at the middle of the filter, so that each half of the FPA is covered by one of the bands. Since the radiation does not arrive only from the direction normal to the filter, the pixels in the middle of the FPA contain radiation that have passed through both filters, so that a group of approximately 80 columns do not contain radiation in only one of the band, but in both of them. This effect, together with the difference of energy arriving to the microbolometer in both bands for a uniform temperature FoV, is appreciated in Figure 3.

### 2.3 Shutter and case

In order to allow or block the entrance of radiation from the FoV, the infrared camera includes a shutter. It has a circular shape, and is placed between the filters and the lenses, attached to an Al case surrounding the filters and the microbolometer.

### 2.4 Optical system & External window

The optical system, consists of a set of lenses that provides a full diagonal 45° FoV. It has a transmittance of about 95 % in the 7 $\mu$m to 14 $\mu$m range.

The outermost layer of the infrared camera system is, as shown in Figure 1, the external window. It is composed of Germanium, and its optical properties must be taken into account before

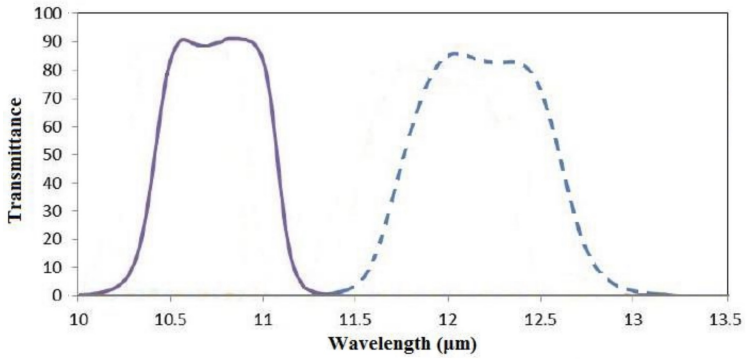


**Figure 2:** Transmittance of the two bands of the filter.

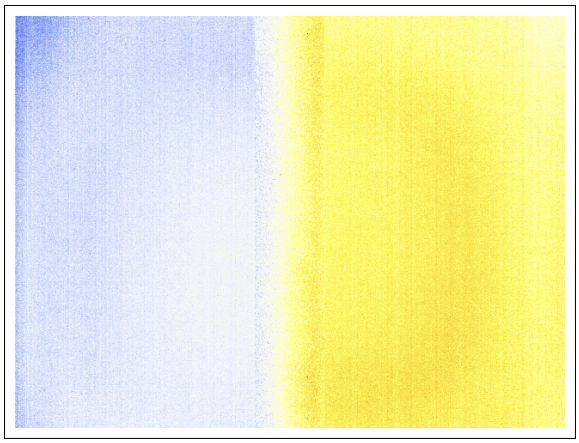

**Figure 3:** Response of the FPA in the two bands and effect of the filters overlapping.

performing any analysis of the data. As it has been explained above, the measure of thermal radiation coming from the objects in the FoV, such as clouds, involve several complex processes along the travel of photons from the external part of the system, trough the external window, the lenses and the filter, until they arrive to the microbolometer. Moreover, apart from affecting the passage of radiation through the whole system, some of the components, such as the shutter and the shutter case, are also big contributors to the radiation arriving to the FPA. A calibration process has been performed to study all these effects and to provide the mechanisms to remove the undesired ones.

## 3. Infrared Camera performance during the flight

The data acquisition electronics, thermal control elements, mechanical devices, power supply and infrared imaging devices inside the infrared camera system worked in a stable and reliable way, making possible the recovery of the hardware together with the data acquired in perfect conditions.

According to the balloon movement through the atmosphere and some parameters of the infrared camera system, the infrared data can be divided in several groups of images which are, according to theses conditions, useful or not for the analysis. The flight is divided in several stages according to the variation of these parameters, as shown in Figure 4.

Due to the programmed working time interval, the infrared camera started the image acquisition just when the balloon took off, and stopped it after the gondola was recovered from the lake where it splashed down. According to this, roughly half of the images were taken under water. Although these data is not adequate for CTH analysis, the relevance in the analysis of the performance of the infrared camera is crucial.

In Figure 5 the external Ge window temperature is shown. As stated in §2.4, its temperature has also a great significance in the analysis of the infrared images. On the contrary of what happens with the shutter temperature, which is controlled in three levels, the external window has a continuous variation, due to the varying atmospheric conditions during the flight. In Figure 5 it is shown the continuously decreasing temperature during the rise, a sharp variation while the balloon was falling down, and then a fast warming until it reached the thermal equilibrium with the water.

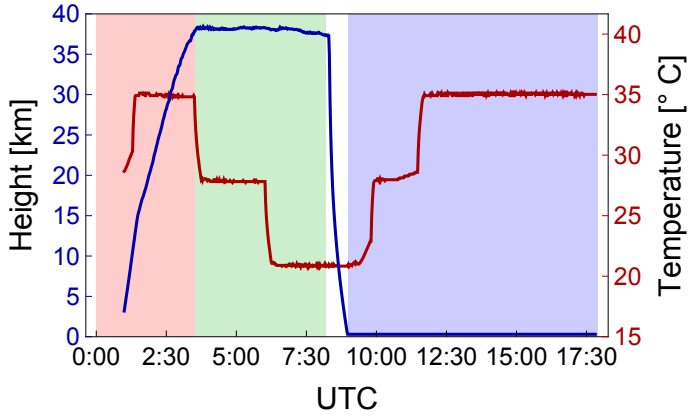


**Figure 4:** Infrared camera flight phases: In red, the rise up, in green the $\sim 40$ km flight, and in blue the under-water region. The height values (blue line) follow the left side ticks, and the temperature of camera shutter (red line), the right ones.

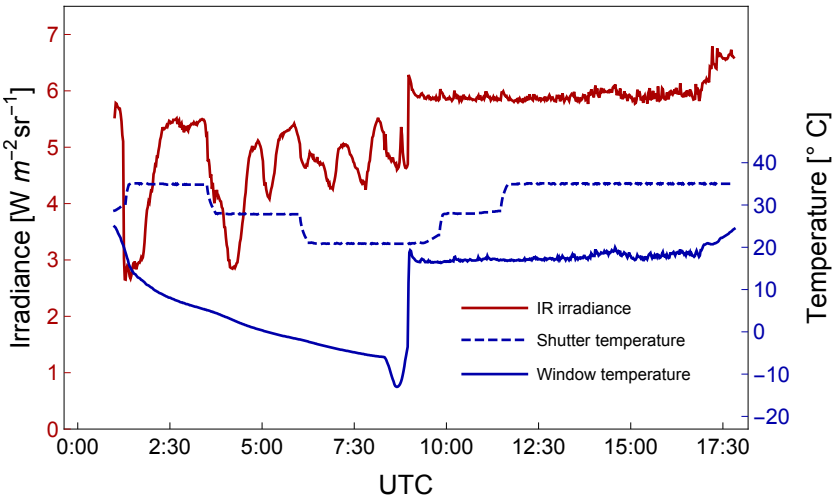


**Figure 5:** Measured irradiance and temperature of the components affecting the FoV. The irradiance values (red line) follow the left side ticks, and the temperatures (red lines), the right ones.

In order to see how these temperatures (the one of the shutter and the one of the external window) affect the amount of radiation reaching the focal plane array, in Figure 4 can also be seen the average irradiance along the FoV during the flight. The effect of window and shutter temperatures must be removed using the calibration data. As can be seen, the irradiance does not show sharp variations where shutter temperature does, nor a tendency to decrease while the window temperature decreases.The short time scale variations observed until the splash down are due to the presence or lack of clouds in the FoV changing, then, the measured irradiance.

Many other electronic parameters required to be in given ranges to ensure the proper behaviour of the system were monitored. Figure 6 contains the temperatures of the battery pack, the acquisition board and the thermo electric cooler of the microbolometer, both in the proper working range. Internal pressure and relative humidity inside the mechanical box are shown in Figure 7 as well.

As stated before, the data acquired while the camera was under water can be used to study the

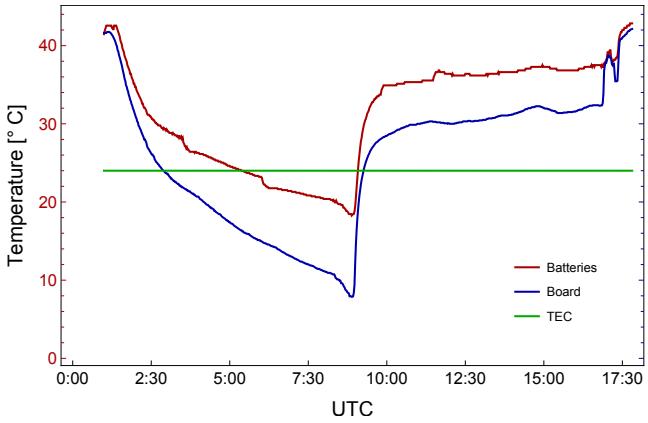


**Figure 6:** Temperatures of the battery pack, the acquisition board and the thermo electric cooler.

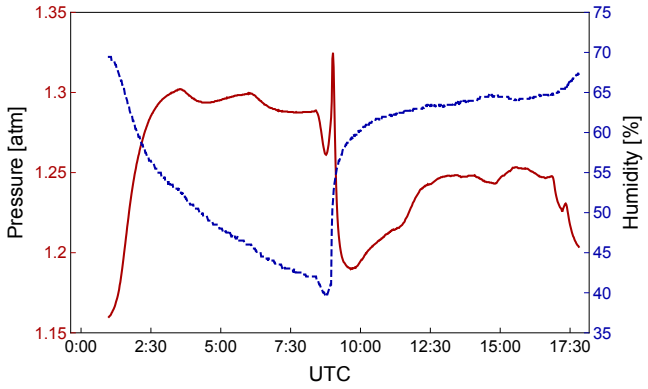


**Figure 7:** Pressure and relative humidity inside the infrared camera box during the flight.

performance of the camera. Firstly, one can analyse the uniformity of the FoV in each filter. This uniformity can be appreciated in Figure 3, after applying the geometrical corrections due to the non-uniformities produced by the optics.

In order to study the statistical accuracy of the infrared camera, the deviation of the irradiance values along the whole FoV (for each band) can give an estimation of the uncertainties in the measures. The distribution of irradiances along the whole FoV for a single under-water image is shown in Figure 8. The data is fitted to two gaussians, providing $\mu_1 = 5.79\ \mathrm{W\,m^{-2}\,sr^{-1}}$, $\sigma_1 = 0.07\ \mathrm{W\,m^{-2}\,sr^{-1}}$, $\mu_2 = 6.02\ \mathrm{W\,m^{-2}\,sr^{-1}}$ and $\sigma_2 = 0.06\ \mathrm{W\,m^{-2}\,sr^{-1}}$ as mean and standard deviations for both filters, providing relative uncertainties of 1%, approximately.

This procedure is repeated for the whole set of images taken under water. The results are shown in figure 9, where the uncertainty is estimated to be, roughly, 1% for all the range. The sharp variation arround 11:30 corresponds to the last variation of the shutter temperature seen in 5.

## 4. Conclusions

The infrared camera system, one of instruments of the EUSO-Balloon experiment has been a

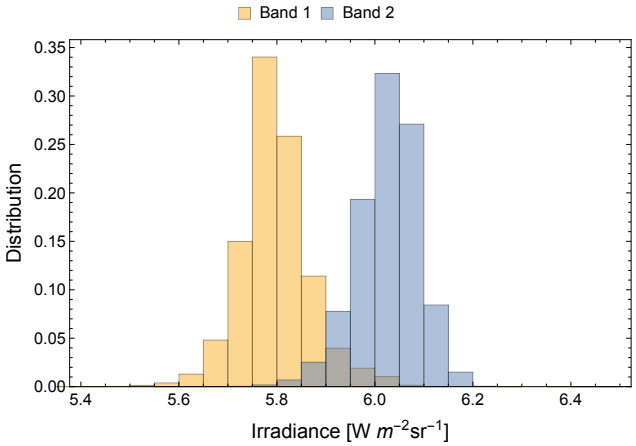


**Figure 8:** Distribution of irradiances along the FoV.

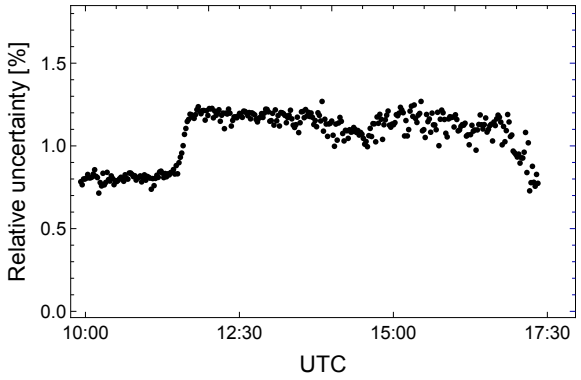


**Figure 9:** Estimated relative uncertainties for under-water images.

complete success as a pathfinder for the space mission for several aspects:

- its battery pack and power supply worked uniformly until the end of the flight,
- the acquisition electronics hardware, and the onboard software, both built specifically for this experiment, worked as expected, making possible the monitoring of the whole system during the flight and the correct acquisition images from the camera,
- the infrared camera, worked properly, providing the measures in both bands along the whole FoV,
- the data analysis is giving the results as was expected, in well agreement with the calibration done before the flight, and being able to remove all the negative effects described here, to discriminate the radiation coming from objects in the field of view, such as clouds, ground and water, and from the objects that compose the measurement decive.

**Acknowledgment:** This work is supported by the Spanish Government MICINN & MINECO under projects AYA2009-06037-E/AYA, AYA-ESP 2010-19082, AYA2011-29489-C03-01 and AYA2011-29489-C03-02, AYA-ESP2012-39115-C03-01 and AYA-ESP2012-39115-C03-03, AYA-ESP 2013-47816-C4, MINECO/FEDER-UNAH13-4E-2741,

CSD2009-00064 (Consolider MULTIDARK) and by Comunidad de Madrid under projects S2009/ESP-1496 & S2013/ICE-2822. The calculations were performed using the Space and Astroparticle SPAS-UAH Cluster. J.A. Morales de los Ríos wants to acknowledge the financial support from the UAH-FPI grant and the RIKEN-IPA program. M. D. Rodríguez Frías acknowledges the Swiss National Science Foundation (SNSF) for a Sabbatical research stay at the University of Geneva. L. del Peral acknowledges a senior grant for a Sabbatical stay at University of Geneva from the Spanish Ministerio de Educación, Cultura y Deporte under the "Salvador de Madariaga Programa Estatal de Promoción del Talento y su Empleabilidad en I+D+i, Subprograma Estatal de Movilidad del Plan Estatal de Investigación Científica y Técnica y de Innovación 2013-2016" M D Rodriguez Frias acknowledges a grant under the "Atraccio de Talent" program from the Vicerrectorado de Investigación de la Universidad de Valencia (Spain).

## References

[1] J.H. Adams *et al.* (JEM-EUSO Collaboration). An evaluation of the exposure in nadir observation of the JEM-EUSO mission. *Astropart.Phys.*, **44**, 76-90, (2013).

[2] The JEM-EUSO Collaboration. The JEM-EUSO Mission: Contributions to the ICRC 2013. *Proc. of 33rd ICRC* ArXiv:1307.7071, (2013).

[3] M. D. Rodríguez Frías *et al.* for the JEM-EUSO Collaboration. The JEM-EUSO Space Mission: Frontier Astroparticle Physics at ZeV range from Space. Homage to the Discovery of Cosmic Rays. *Nova Science Publishers, New York*. ISBN: 978-1-62618-998-0, Inc, pg 201-212, (2013).

[4] The JEM-EUSO Collaboration (corresponding authors: S. Toscano, J. A. Morales de los Ríos, A. Neronov, M. D. Rodríguez Frías & S. Wada). The Atmospheric Monitoring System of the JEM-EUSO instrument. *Experimental Astronomy*, **37**, (2014),

[5] M. D. Rodríguez Frías, S. Toscano, E. Bozzo, L. del Peral, A. Neronov and S. Wada for the JEM-EUSO Collaboration. The Atmospheric Monitoring System of the JEM-EUSO Space Mission. *Proceedings of the 2$^{nd}$ AtmoHEAD Conference*, (2014).

[6] M. D. Rodríguez Frías *et al.* for the JEM-EUSO Collaboration. The Atmospheric Monitoring System of the JEM-EUSO Space Mission. *Proc. International Symposium on Future Directions in UHECR Physics, The European Physical Journal*, **53**, 10005, pg1-7, (2013).

[7] The JEM-EUSO Collaboration (corresponding authors: J. A. Morales de los Rios & M. D. Rodríguez Frías). The infrared camera onboard JEM-EUSO. *Experimental Astronomy*, **37**, (2014).

[8] J. A. Morales de los Ríos, E. Joven, L. del Peral, M. Reyes, J. Licandro and M. D. Rodríguez Frías. The Infrared Camera Prototype Characterization for the JEM-EUSO Space Mission. *Nucl. Instr. Meth. Phys. Res. A*, **749**, 74-83, (2014).

[9] M. D. Rodríguez Frías *et al* for the JEM-EUSO Collaboration. Towards the Preliminary Design Review of the Infrared Camera of the JEM-EUSO Space Mission. *Proc. of 33rd ICRC* , (2013).

[10] A. Merino *et al.* for the JEM-EUSO Collaboration. Cloud Top Height estimation from WRF model: Application to the IR camera onboard the EUSO-Balloon (CNES). *Proc. of 34th ICRC*, #0979 (2015).

[11] P. von Ballmoos *et al.* for the JEM-EUSO Collaboration. A balloon-borne prototype for demonstrating the concept of JEM-EUSO. *Adv. Space Res.* **53** (2014) 1544-1550.

[12] G. Sáez-Cano *et al.* for the JEM-EUSO Collaboration. Cloud Optical Depth obtained from the Spanish Infrared Camera data and the Laser shots of the USA helicopter during the EUSO-Balloon (CNES) flight. *Proc. of 34th ICRC*, #1024 (2015).